Journal of Power Sources 418 (2019) 176–185

Contents lists available at ScienceDirect

Journal of Power Sources

journal homepage: www.elsevier.com/locate/jpowsour

State of charge dependency of the overvoltage generated in commercial Li-ion cells

V.J. Ovejas*, A. Cuadras

Grup de Processat d'Energia i Circuits Integrats (EPIC), Departament d'Enginyeria Electronica, Escola d'Enginyeria de Barcelona Est EEBE, Universitat Politècnica de Catalunya - BarcelonaTech, Barcelona, Spain

HIGHLIGHTS

- Overvoltage is tracked with respect to SoC during galvanostatic discharge.
- Contributions to overvoltage are identified from half-cell measurements.
- We find experimentally a relation between diffusion and phase transitions.
- Diffusion decreases at the initial stages of a phase formation.
- Overvoltage is found to be more appropriate than ICA in full cell measurements.

GRAPHICAL ABSTRACT

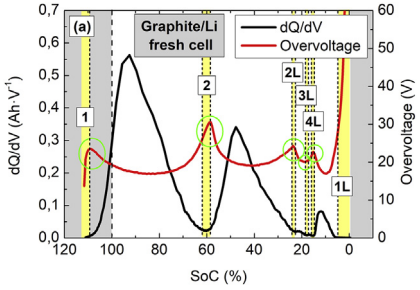

ARTICLE INFO

Keywords:
Overvoltage
Activation polarization
Concentration polarization
Phase transformation
NMC
Half-cells

ABSTRACT

The overvoltage that is produced in the cells under operation limits the capacity and power they can deliver. A detailed study about the mechanisms that contribute to that overvoltage—and thus to their lifetime—is required for optimizing the use of batteries as well as their manufacturing process.

We investigate galvanostatic discharge at low and moderate rates in an LCO-NMC/graphite cell in order to quantify the ohmic voltage drop and activation and concentration polarizations. For doing so, we compare half-cells to full cell overvoltages. We find that the ohmic drop and concentration polarization dominate at high rates and low rates, respectively. Moreover, we track the evolution of concentration polarization with State-of-Charge (SoC) and we observe that there exists a relationship between diffusion and phase transformations. Specifically, we validate experimentally that initial stages of a phase formation are not dominated by diffusion. Phase transitions are commonly evaluated by incremental capacity analysis. However, we determine that it is more appropriate to obtain that information from the full cells by the overvoltage analysis. Furthermore, we suggest that the working SoC range can be optimized from the overvoltage analysis by avoiding the particular SoCs at which the most detrimental phase transitions take place.

1. Introduction

Li-ion batteries are widely accepted as power sources for an increasingly number of portable applications ranging from cellphones to electric vehicles. Their high energy and power densities make them the more appropriate solution for portable devices. However, their performance is compromised as long as they are used in any dynamic or stationary application (cycling or storing energy) due to the degradation or wear out that they suffer.

Currently, battery performance is characterized by the capacity and power the cells can deliver for given conditions. In fact, for a certain application, capacity fade and/or power fade determine the cells

* Corresponding author. Campus Diagonal Besòs, Edifici A (EEBE-UPC), Av. Eduard Maristany, 16, 08019, Barcelona, Spain.
E-mail addresses: victoria.julia.ovejas@upc.edu (V.J. Ovejas), angel.cuadras@upc.edu (A. Cuadras).

https://doi.org/10.1016/j.jpowsour.2019.02.046
Received 25 July 2018; Received in revised form 24 January 2019; Accepted 13 February 2019

lifetime. Capacity and power are commonly determined from voltage and current measurements [1,2]. Thus, voltage as much as current are critical magnitudes for determining the cells performance. However, the current to voltage relation in Li-ion batteries is complex and depends on many external and internal factors such as temperature, the geometry of the cell and its components, current density, State-of-Charge (SoC), or the aging level [3].

In an electrochemical cell, the available electrical energy can be calculated from the change in Gibbs free energy of the electrochemical couple [4].

$$\Delta G = -n \cdot F \cdot OCV \tag{1}$$

where *OCV* stands for Open Circuit Voltage (cell voltage when the cell is at chemical equilibrium), n is the exchanged number of electrons in the reaction, and F is the Faraday constant (96487 C mol^{-1}).

Unfortunately, all the available electrical energy when the cell is at equilibrium cannot be converted into useful electrical energy because some of it is lost when a current flows through the cell; the cell potential (V_{cell}) deviates from the open circuit voltage reducing the amount of energy that can be converted. This voltage deviation is usually termed as overvoltage (η) (or undervoltage depending on the direction of current but, in this contribution, it will be always referred as overvoltage independently of the direction of current) [5]:

$$\eta = OCV - V_{cell} \tag{2}$$

The overvoltage generated in the cells during charge or discharge is caused by electronic conduction, ionic mass transport, and charge transfer phenomena [6,7]. In fact, overvoltage represents the energy dissipated as heat during these transport and transfer phenomena. It is well known that all the irreversible processes dissipate energy; dissipation (or overvoltage in our case) can be used as an indicator of the irreversibility of a system [8–10]. Thus, it is expected that the cells will become more inefficient by dissipating more energy (i.e. the overvoltage will increase) as they age or degrade (decrease their reversibility) [11]. The larger the overvoltage is the sooner the charge/discharge cut-off voltage is going to be reached. Thus, limiting the capacity (the amount of charge that can be inserted/extracted) and the power capabilities of the cells. In general, the contributions to overvoltage can be classified in ohmic and non-ohmic effects. The part associated to ohmic conduction is usually termed as ohmic drop [11]. It is a purely resistive effect and therefore shows a linear relationship between current and voltage, following the Ohm's law, at any current. The physical origin of the ohmic drop comes from the contributions of the ionic resistance of the electrolyte and the electronic resistances of the active mass, the interfaces between electrodes and current collectors, and the electrical tabs [12].

The part of overvoltage that is non-ohmic is associated to polarization loses and includes activation and concentration polarizations. Activation polarization drives the electrochemical reaction at the electrode surface and is related to a charge transfer process. The associated overvoltage (η_{CT}) comes from the energy required to overcome the activation barrier for the chemical reaction to take place [12,13]. In particular, the dynamics of activation polarization follow the Butler-Volmer equation (3) [14].

$$I = I_a + I_c = i_o \cdot \left[e^{\frac{(1-\alpha)\cdot n \cdot F \cdot \eta_{CT}}{R \cdot T}} - e^{-\frac{\alpha \cdot n \cdot F \cdot \eta_{CT}}{R \cdot T}} \right] \tag{3}$$

where I represents the net current flowing in the cell, I_a is the anodic current, I_c the cathodic current, i_o the exchange current (current flowing at each of the electrodes when the cell is at equilibrium, when the net current is zero), α the electron transfer coefficient, R the gas constant, and T the temperature at which the reaction takes place.

Two simplifications of the Butler-Volmer equation are commonly found; for small voltages, it is linearized and for large voltages, current and overvoltage are related through a logarithmic function [15]. In the first case, the activation overvoltage can be directly obtained from impedance measurements (from charge-transfer resistance R_{CT}), in which a linear relation between current and voltage is assumed (4) [16].

$$\eta_{CT} = -\frac{R \cdot T}{n \cdot F \cdot i_0} \cdot I = R_{CT} \cdot I \tag{4}$$

Contrarily, in the second case in which cells are working at high rates, overvoltage and current do not follow anymore the linear approximation. Therefore, charge-transfer resistance at high rates depends on the applied current (5) [6,16–18].

$$\eta_{CT} = -\frac{R \cdot T}{\alpha \cdot n \cdot F} (\ln i_0 - \ln i) \tag{5}$$

The other non-ohmic term, which is concentration polarization or diffusion overvoltage (η_{diff}), is caused by spatial variations in reactant concentration that can take place in the electrode (solid phase) or in the bulk of the electrolyte (liquid phase) [19]. Those variations at the solid phase are usually associated to the fast consumption of reactants during the electrochemical reaction compared to the rate at which they can diffuse into the electrode particles. In that situation, the transport of lithium-ions inside the active material particles is driven by the concentration gradient that is formed between the surface of the particles and their inner part and it is termed as solid-state diffusion [15]. Solid-phase concentration polarization depends on the applied current, the structure of the active material, temperature and particle size [15]. Conversely, concentration polarization or diffusion at the liquid phase takes place at the electrolyte, which is located between the two current collectors. In particular, it depends on salt concentration, which is affected by the properties of the electrolyte itself, the porosity and the tortuosity of the electrodes [11]. Commonly, concentration polarization is low at the beginning of discharge but grows rapidly for high current loads or towards the end of discharge [19]. Therefore, the total overvoltage generated in a cell under operation, can be written as the charge transfer and diffusion overvoltages of both electrodes plus the ohmic conduction [5]:

$$\eta = [(\eta_{CT})_a + (\eta_{diff})_a] + [(\eta_{CT})_c + (\eta_{diff})_c] + I \cdot R_\Omega \tag{6}$$

where, the subscripts a and c stand for “anode” and “cathode” respectively, and R_Ω is the ohmic resistance of the cell.

The generated overvoltage in the cells depends on the SoC at which they are evaluated [20,21]. Overvoltage reflects transport phenomena and transport depends on the composition of the cells, which is continuously changing during charge and discharge processes. In particular, Li-ion batteries are composed of insertion or porous electrodes in which lithium ions intercalate and deintercalate during charge and discharge processes. Under these circumstances, the materials composing the electrodes undergo various phase transformations depending on their lithium composition [21–27]. The occurrence of these phase transitions depend on many parameters such as temperature, charge/discharge rates, the particle size of the active materials, or the applied overvoltage [21–27]. In general, in the literature, there are many studies dealing with the dependence on the applied overvoltage of the formation of certain phases [21,22,24–27]. However, fewer research works evaluate the overvoltage that is generated in the cells when they are discharged at a constant current [22]. In general, phase transitions are evaluated using complex crystallographic techniques such as XRD, when the cells are at equilibrium. Other techniques commonly employed for studying the dynamics of phase transitions are incremental capacity analysis (ICA) or voltammetric techniques. However, ICA requires a deep knowledge of the electrochemical behavior of the cells [1], previous half-cell measurements in order to decipher the results [28,29], and voltammetric techniques require a sweep of the applied voltage versus time [30,31]. Thus, at present, no information of phase transitions can be extracted when the cells are *in operando*. Moreover, dynamics of the electrodes are, in general, poorly understood [4].

It is important to track the evolution of phase transformations for a

proper characterization of the cells and understanding of the aging process. Phase changes can reveal very valuable information about the internal state of the cells as well as their thermodynamics and kinetics because they are directly related to the physical processes involved in the lithium insertion and extraction [32,33]. Thus, information extracted from these data can also be very useful in first, to build cells that can operate more efficiently and second, to determine the working voltage range (i.e. SoC range) that would optimize the lifetime of the cells [33]. For instance, some of the phase transformations have associated a large volume change that is not beneficial for the cyclability of the cells [32].

In this paper, we present the overvoltage dependency on SoC at two different aging states in an LCO-NMC/graphite cell subjected to a galvanostatic discharge. Then, we determine the various overvoltage sources participating in the overvoltage production. For doing so, the tendencies of half-cell overvoltages are also evaluated and subsequently related to the full cell. Beyond that, we find a relationship between the overvoltage (in particular, concentration polarization) and phase transformations taking place during lithium insertion/extraction. Finally, in contrast to what happens with incremental capacity analysis in full cells with complex peak patterns such as NMC/graphite, we are able to identify all the phase formations in the full cell by simply observing the overvoltage curves. We would like to highlight that regard we are representing data at two different aging levels, the aim of this research work is not to find an aging model according to the generated overvoltage.

2. Experimental

The evaluated cells are commercial 2.8 Ah Li-ion cells supplied by LG_Chem in a 18650 format. Positive electrode (PE) and negative electrode (NE) are composed of $LiCoO_2$ - $Li[NiMnCo]O_2$ (or LCO-NMC) and C_6 (or graphite), respectively.

2.1. Cycle aging procedure

In order to evaluate the cells at various aging levels, they were subjected to a cycle-aging process. They were charged at constant-current/constant-voltage at a C/2 rate and discharged at constant current at a 3C/2 rate, which is the maximum discharge current allowed by the manufacturer. Cycling was performed in an HVBT 5560 Arbin Tester capable of measuring current and voltage. Tests were carried out in a climatic chamber at 25 °C.

Prior to the cycle-aging test, the cells underwent six formation cycles at 25 °C to stabilize their capacity and to allow the initial formation of the Solid-Electrolyte Interface (SEI) layer. Thus, we consider the cells are fresh right after the formation cycles (fresh cells) and aged at the end of the cycle-aging procedure (aged cells) The capacity fade suffered by the aged cell at a 3C/2 discharge rate was of 24% with respect to the nominal capacity. A more detailed description of the aging process can be found in Ref. [34].

2.2. Half-cells building procedure

Cell opening was performed at the Institute for Power Electronics and Electrical Drives (ISEA) in Aachen (Germany). Further details can be found elsewhere [34]. Cell opening was carried out to one fresh cell after the formation cycles (fresh cell) and one aged cell after the cycle-aging process (aged cell) (Section 2.1). Round samples of 16 mm diameter were harvested from positive and negative electrodes of fresh and aged cells.

In order to build the half-cells, one of the active material sides of the harvested samples had to be previously removed. It was done by applying *N*-Methyl-2-pyrrolidone (NMP) solvent by hand until the active material detached from the current collector. In particular, half-cells were built in a coin cell format introducing the harvested positive or negative electrode, fresh separator, 90 μL of fresh electrolyte and metallic lithium as the counter electrode.

2.3. Open circuit voltage

In this work, OCV is estimated from cell voltage measurements at very low charge/discharge rates—in particular C/25—because at low C-rates, kinetic effects are minimized, and thus, thermodynamic contribution dominates the measured voltage response. Therefore, those voltage curves can be related to the SoC and can be used to estimate the OCV [35]. The estimated pseudo-OCV (ps-OCV) is calculated at every SoC by averaging the measured charging and discharging voltages obtained at those low rates. Voltage measurements were carried out to fresh and aged cells with an HVBT 5560 Arbin Tester at 25 °C.

2.4. Overvoltage generated in the cells

The overvoltage generated in the cells under operation was determined at C/25 and 3C/2 discharge rates by equation (2) in fresh and aged cells. Voltage and current measurements were carried out with an HVBT 5560 Arbin Tester at 25 °C.

In the linear working regime of the cells, the overvoltage can be related to the corresponding resistance (R) and current [5]:

$$\eta = I \cdot R \tag{7}$$

Thus, in order to determine the various contributions to overvoltage, we employed the results of the impedance analysis we carried out in a previous work [36]. Moreover, we could discriminate the various contributions to overvoltage (ohmic, activation and concentration polarization terms) because we measured the impedance of half-cells we build during a post-mortem analysis [34].

2.4.1. Activation polarization

In the case of activation polarization, a distinction is made between the cases in which the cells are working at small overvoltages (linear approximation) and the cases in which the logarithmic approximation is more appropriate (refer to Section 1). In the linear approximation, the overvoltage related to charge transfer is obtained by equation (4), which in that case is equivalent to (7). Nevertheless, in the case of the logarithmic approximation, the overvoltage determination is not as straightforward as it is in the linear case so some intermediate steps are required. The procedure we followed is, first, to calculate the exchange current from the impedance data by the use of equation (4), as it does not depend on the rate but it does on the electrode composition or the SoC [37]. Once i_0 is calculated from the impedance data at every SoC, activation polarization can be calculated with equation (5). In this study, as no experimental data was available for the electron transfer coefficient, symmetric electron transfer was assumed ($\alpha = 0.5$) as it is referred in the literature as a good approximation to experimental data [38].

2.4.2. Concentration polarization

The contribution of concentration polarization is obtained from equation (6) because the resistance associated to that term was not measured in Ref. [36]. Thus, concentration polarization (η_{diff}) is obtained as the difference between the total overvoltage (η), and the addition of ohmic (η_Ω) and activation (η_{CT}) contributions (8).

$$\eta_{diff} = \eta - (\eta_\Omega + \eta_{CT}) \tag{8}$$

2.5. Determination of the state of charge

SoC is defined as the ratio of the remaining charge to the actual capacity of the cell. The capacity of the cells has to be measured at very low rates in order to minimize the kinetic limitations. Likewise, capacity depends on the voltage window at which we operate the cell, the

Table 1
Voltage windows and C-rates at which the SoC was determined in the full cells and half-cells.

Cell	Minimum voltage (V)	Maximum voltage (V)	C-rate	Parameter
Full cell LCO-NMC/C_6	3	4.3	C/25	SoC
Half cell LCO-NMC/Li	3	4.4	C/25	PE SoC
Half cell C_6/Li	0.00075	2.5	C/25	NE SoC

rate at which it is measured and the temperature of the cell [3,39].

Capacities of full cells and half-cells were measured at room temperature at a charge/discharge rate of C/25 (Table 1). In particular, capacities of full cells were measured with an HVBT 5560 Arbin Tester and half-cell capacities were measured with a BasyTec battery tester.

The voltage window that we selected for cycling the half-cells has not to necessarily correspond to the actual voltage window at which the electrodes work in the full-cell configuration. Furthermore, the matching of the electrodes also varies during the lifecycle of the cells due to the degradation mechanisms that take place, such as loss of lithium or loss of active material [40]. Thus, we obtained the equivalence between half-cells and full cell SoCs through the adjustment of the voltage curves along with the injected/extracted charge.

2.6. Incremental capacity analysis

Incremental Capacity Analysis (ICA) was carried out during a discharge process at C/25. Thus, the extracted charge was represented versus the measured voltage curves. At that point, incremental capacity was obtained as the portion of capacity associated to every voltage step ($\Delta Q/\Delta V$). Peaks at the incremental capacity curves represent the coexistence of distinct phases (represented as plateaus at the thermodynamic voltage curves). Every chemistry has a characteristic peak pattern and each peak at the incremental capacity curve has a unique shape and a particular intensity. Contrarily, changes in slope in the thermodynamic voltage curve (transitions between plateaus) are related to the formation of pure phases [25,35,41,42]. Those phases can be structured, in the particular case of Li-ion cells, as dense or liquid-like solid structures [22].

Incremental capacity analysis is a very powerful technique to investigate changes in the electrochemical properties of the electrodes. It allows to quantify aging and to differentiate loss of lithium, loss of active material and polarization effects [35,43,44].

3. Results and discussion

In this section, we first present the results of the generated overvoltage at two discharge rates and at two aging levels. Then, we discriminate the various contributions that participate in generating this overvoltage and we determine the overvoltage produced at each of the electrodes by means of half-cells. In addition, we perform an incremental capacity analysis that allows us to find a relationship between phase transitions and overvoltage. Finally, ICA and overvoltage curves are compared as methods for determining the evolution of phase changes in full cell configurations.

3.1. Overvoltage in full cells during a galvanostatic discharge

In order to determine the overvoltage, the open circuit voltage has to be known (2). Pseudo-OCV (refer to Section 2.3) is estimated in fresh and aged cells (Fig. 1). Slightly variations between the OCV curves are appreciated at some SoCs, which are attributed to the degradation suffered by the cells during the cycle-aging process [34].

Cell voltages of fresh and aged cells have been measured at C/25 (Fig. 2a) and 3C/2 (Fig. 2b) discharge rates. What we observe is that at

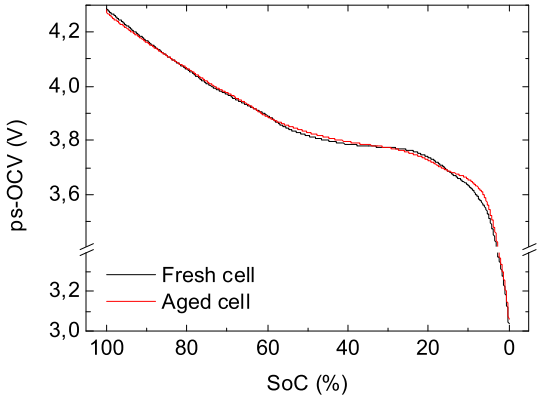

Fig. 1. Pseudo-OCV of fresh and aged cells obtained at room temperature by averaging charge and discharge voltage curves at a low rate (C/25).

3C/2 there is a noticeable increase in the ohmic drop between fresh and aged cells (Fig. 2b). This increase in the initial voltage losses coincides with our previous results in which the ohmic resistance was the most affected part due to aging [36]. Moreover, it can be appreciated that there is also a larger difference between the voltage curves of the fresh and the aged cells at SoCs below 40% (Fig. 2b). In contrast, in the voltage curves at C/25, only slight differences can be appreciated (Fig. 2a).

The corresponding overvoltages at C/25 (Fig. 3a) and 3C/2 (Fig. 3b) are obtained by combining ps-OCV curves (Fig. 1) and cell voltages under polarization (Fig. 2), as it is expressed in equation (2). In general, we find that the overvoltage increases as the rate increases and as the cells age. Similar tendencies are also found in Refs. [11,45,46], respectively. Apart from the increase in overvoltage due to aging (Fig. 3) the curves also become softer, showing an increase in overvoltage at SoCs in which it tended to decrease when the cells were fresh. For instance, at SoCs around 15–20% or 75% at a C-rate of 3C/2, and around 60% at C/25. In addition, it can be appreciated that the overvoltage increases or decreases depending on the evaluated SoC (Fig. 3). A decrease in overvoltage at some particular SoCs is also appreciated in the simulations made by Chandrasekaran, but no explanation is given in this work [11].

3.2. Ohmic, activation and concentration polarizations

In this section, we first analyze the overvoltage contributions of the ohmic conduction (current collectors are separated from the rest of ohmic contributions), charge transfer at positive electrode, and conduction through the SEI layer (Fig. 4). These effects (their impedance contributions) were already identified in our previous research work [36] (refer to Subsection 2.4). The ohmic overvoltage contributions are obtained by the product of their associated resistances and the discharge current (7) whereas a different approximation is carried out in the particular case of activation polarization (refer to Section 2.4.1). Once ohmic conduction and activation polarization are determined, concentration polarization is obtained by equation (8) and is plotted along with the other effects (Fig. 5).

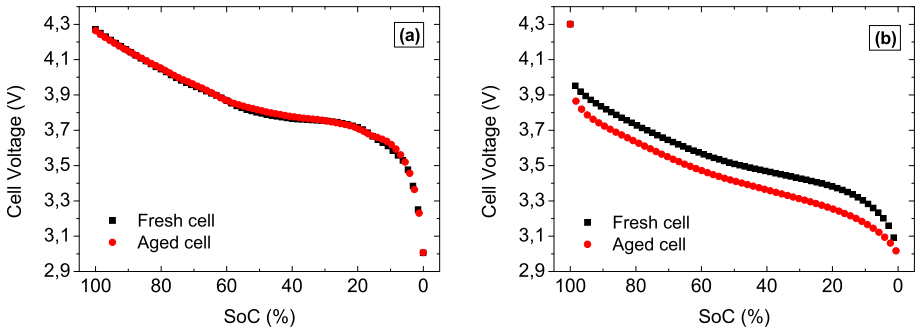

Fig. 2. Cell voltages of a fresh and an aged cell at room temperature at (a) C/25 and (b) 3C/2 discharge rates. Results are represented with respect to SoC.

We find that the maximum contributor to overvoltage at both low and moderate discharge rates is the term associated to *other ohmics*—that corresponds to all the ohmic contributions except current collectors—which include the ionic conduction through the electrolyte and the electronic conduction through the tabs, active material particles, and connections (Fig. 4). In general, the overvoltage associated to electronic conduction can be considered negligible compared to the ionic one [11]. Thus, the largest overvoltage contribution among the ohmic drop, the transport across the SEI, and the activation polarization term might come from the ionic conduction in the electrolyte. Some of the parameters that affect the ionic conduction are salt concentration and the porosity of the electrodes [11,47]. Therefore, the optimization of the porosity of the electrodes and an appropriate selection of the electrolyte is recommended in order to reduce the ohmic loses during galvanostatic discharge.

When the fresh cells are discharged at a C/25 rate, the overvoltages related to the SEI layer and charge transfer at positive electrode are comparable (Fig. 4a). Nevertheless, at the aged state, charge transfer contributes more to total overvoltage than the SEI (Fig. 4b). Contrarily, at a discharge rate of 3C/2, the overvoltage generated in the SEI of the fresh cell is larger than that associated to charge-transfer (Fig. 4c). Thus, the overvoltage generated at the SEI layer is not critical at room temperature but it gains importance as the discharge rate increases. Despite the evident increase in the overvoltage associated to charge transfer in the case of the aged cell, both the SEI and charge-transfer overvoltages contribute in the same amount, except at SoCs below 20% from which charge transfer starts increasing exponentially (Fig. 4d). Thus, as it occurs at C/25, the last stages of discharge are limited by the slowdown of the electrochemical reaction at the positive electrode. Nevertheless, at the highest discharge rate, the cells are limited by ohmic conduction in all the evaluated SoCs, even at the aged state (Fig. 4c and d).

If now we include concentration polarization, which is obtained by equation (8), we observe that it is the responsible of the overvoltage SoC dependency that we find in Section 3.1 (Fig. 5). Concretely, concentration polarization shows sharp increases and drops at some particular SoCs. The most prominent local maxima are located at SoCs around 80%, 60%, 25%, and 10% in the fresh cell when discharged at C/25 (Fig. 5a). In general, we find that these peaks tend to disappear as the rate increases and the cells age, what leads to a more homogeneous distribution of the overvoltage with respect to cells composition (Fig. 5b–d).

In general, we find that concentration polarization contributes mostly at low rates but always tends to increase towards the end of discharge, especially for SoCs below 20% at C/25 (see (Fig. 5a and b) and below 40% at 3C/2 at the aged state (Fig. 5d). In fact, in the last stages of discharge, a sharp decrease in cell voltage is also observed (Fig. 2), which is attributed to the depletion of reactants at the surface of the active material particles [15]. In literature, it is already stated that concentration polarization becomes dominant at later times and high filling [48]. Thus, when the cells are connected to a load during a long period, such as when they are discharged at a C/25 rate, concentration polarization is expected to be one of the major contributors to overvoltage as it is observed (Fig. 5a and b).

At a discharge rate of 3C/2, the ohmic contribution clearly dominates the drift in voltage (Fig. 5c and d). In addition, in the fresh cell, the voltage drop related to the SEI layer gains importance compared to lower rates, getting values comparable to diffusion (around 50 mV) (Fig. 5d). Moreover, as the cells age, activation polarization increases to values comparable to diffusion and the SEI layer (Fig. 5d). Actually, at the end of discharge, which is reached at SoCs around 14% in that case, the overvoltage associated to diffusion increases to values comparable to the ohmic drop (Fig. 5d).

3.3. Overvoltages generated in positive and negative electrodes

We investigate here the overvoltages generated in half-cells. We observe in the fresh cells that the overvoltage generated in the negative electrode is twice the one produced in the positive electrode (Fig. 6a). However, as the cells age, the overvoltage generated in the positive

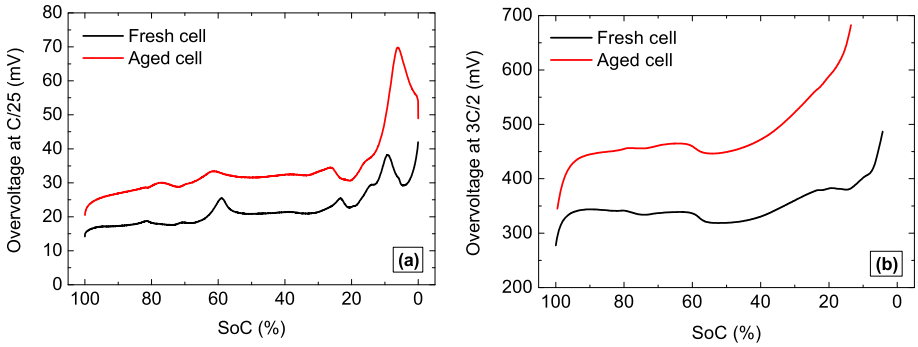

Fig. 3. SoC evolution of the overvoltages generated at room temperature in fresh and aged cells during (a) a galvanostatic discharge at C/25 and (b) a galvanostatic discharge at 3C/2.

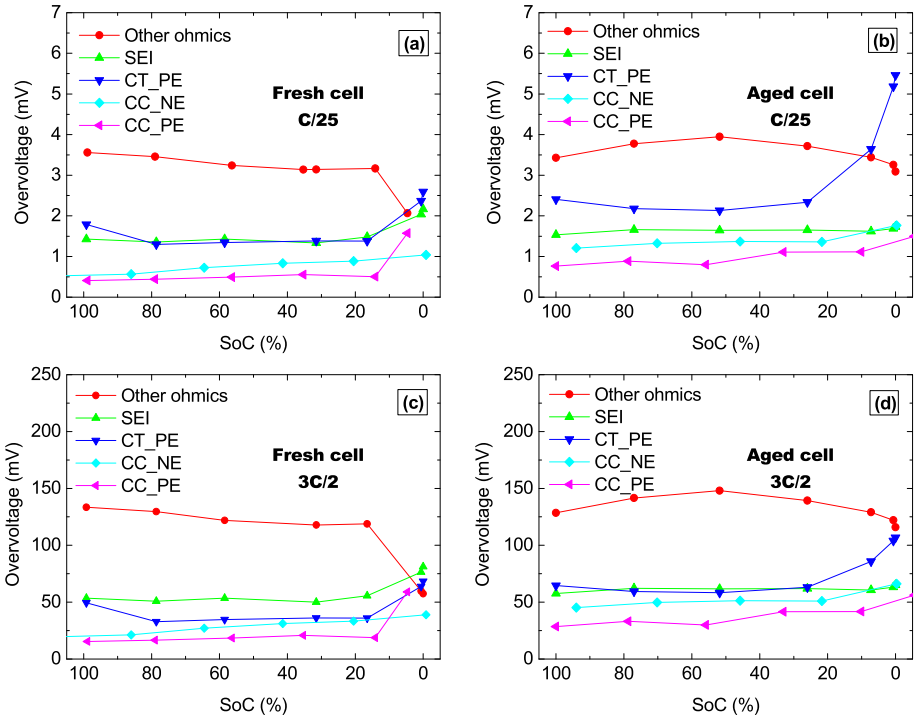

Fig. 4. Overvoltage generated at current-collector interfaces of positive and negative electrodes (CC_PE and CC_NE), at the SEI layer which is formed at negative electrode surface, during charge-transfer at positive electrode (CT_PE) and the rest of ohmic contributions (other ohmics). Overvoltage is evaluated in (a) a fresh cell at a C/25 discharge rate, (b) an aged cell at a C/25 discharge rate, (c) a fresh cell at a 3C/2 discharge rate and (d) an aged cell at a 3C/2 discharge rate. Measurements are carried out at room temperature.

electrode suffers a larger increase than that in the negative electrode, what yields to comparable overvoltages in both electrodes (Fig. 6b). Thus, indicating that the more degraded electrode in terms of overvoltage is the positive electrode.

If the overvoltage generated in the full cell at a C/25 discharge rate (Fig. 5a and b) is compared to the overvoltage generated in the half-cells (Fig. 6a and b), similar peak patterns are observed. Therefore, the electrode causing each of the various peaks observed in the full-cell overvoltage can be discriminated. Specifically, we determine that local maxima in overvoltage at SoCs 81.3% and 10% in the case of fresh cells correspond to positive electrode whereas those at SoCs 58% and 23.5% are produced at the negative electrode (Table 2). Smaller amplitude peaks are also appreciated in the full cell at SoCs around 71% and 39%, which are attributed to the positive electrode, and around 14%, attributed to the negative electrode (Fig. 5a and b, and Table 2). All those peaks shift their SoC position during the aging test due to the various degradation mechanisms that take place (Table 2). Further details concerning degradation mechanisms can be found elsewhere [34].

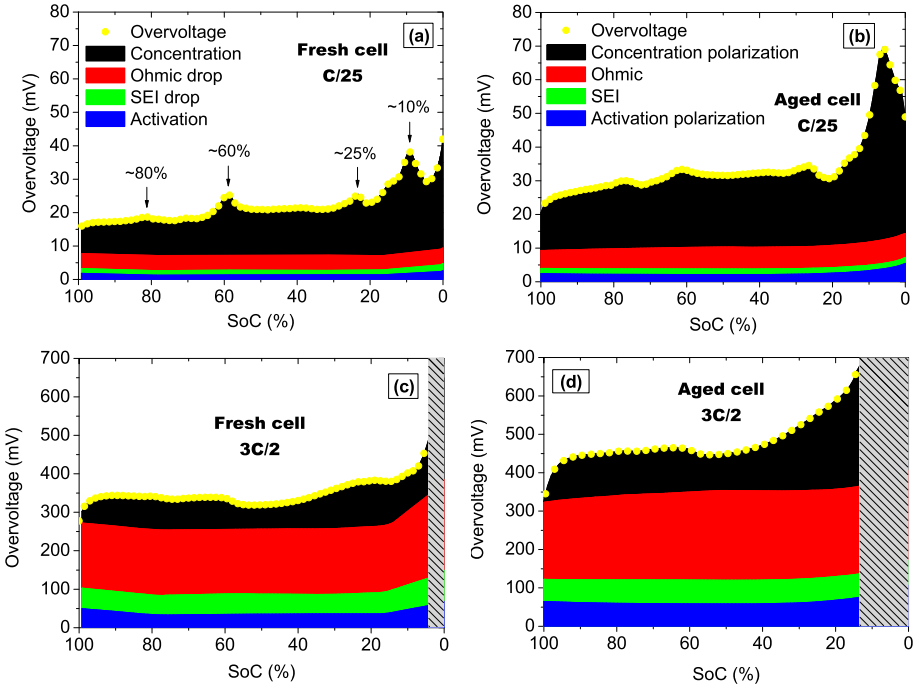

Fig. 5. Various contributions to overvoltage at room temperature and at different discharge rates and aging levels: (a) fresh cell at C/25, (b) aged cell at C/25, (c) fresh cell at 3C/2 and (d) aged cell at 3C/2. Arrows highlight the main overvoltage peaks. Gray areas at low SoCs represent that the end of discharge is reached.

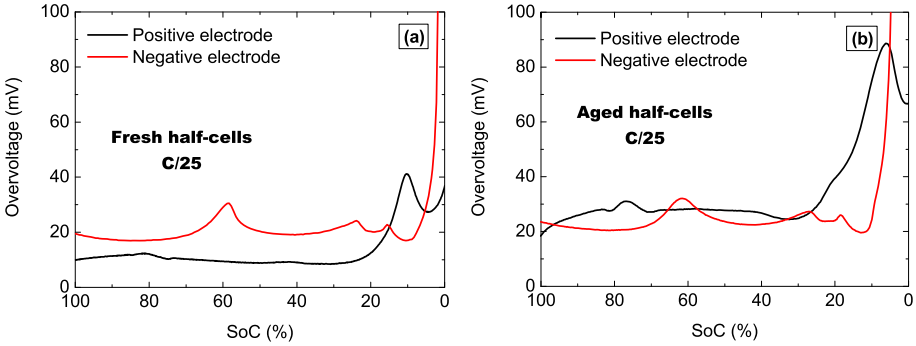

Fig. 6. Overvoltages produced at positive and negative electrode half-cells at a discharge rate of C/25 at room temperature. (a) Half-cells composed of samples harvested from the fresh cell and (b) half-cells composed of samples harvested from the aged cell. Ohmic drop is subtracted from total overvoltage.

Table 2
SoCs corresponding to local maxima in full-cell overvoltages represented in Fig. 5a and b.

Electrode	SoC of the local maxima in fresh cells (%)	SoC of the local maxima in aged cells (%)
Positive	81.3	77
Positive	71	70
Negative	58	61
Positive	39	37.6
Negative	23.5	26.5
Negative	14	15
Positive	10	6

3.4. Relationship between phase transitions and overvoltage

The particular overvoltage SoC dependency that we find in the evaluated NMC cells (Figs. 5 and 6) allows us to establish a relationship between overvoltage and phase transformations during galvanostatic discharge. In order to generalize these results, the same dependency should be validated in other Li-ion chemistries. Actually, the SoC dependency of the overvoltage generated in two commercial LFP cells was already evaluated in a previous work [34]. However, half-cell analyses were not carried out to those cells what did not allow to establish the possible relationship between overvoltage and phase transformations. Nevertheless, we found similar peak patterns in those commercial cells what might indicate that there also exists a relationship between the chemistry (or the phase transitions related to this particular chemistry) and the overvoltage.

Incremental capacity analysis is carried out to the full cell and the half-cells in order to determine the various phase transformations occurring during lithiation of positive electrode and delithiation of the negative one (Fig. 7). Fresh and aged cells are evaluated (left and right sides of Fig. 7, respectively). Results are represented with respect to SoC instead of cell voltage in order to compare them with the generated overvoltages that we have shown in Fig. 3a, Fig. 5a, and Fig. 6.

It is well-known that graphite undergoes five phase transitions during delithiation at room temperature [22,26,28,49–51]. Concretely, staging in graphite during lithium extraction goes from stage 1 to stage 2, and then stages 2L, 3L, 4L and 1L [22]. Every number (1, 2, 3, or 4) represents the interslab in which lithium ions are intercalated. Likewise, ions can be intercalated in every interslab in an ordered manner as it happens in stages 1 and 2 or in a disordered (liquid-like) manner such as 2L, 3L, 4L and 1L [22]. In our study, stages 1, 2, 2L, 3L, 4L, and 1L are clearly identified in the incremental capacity curves in both fresh and aged electrodes (Fig. 7a and b). Moreover, we find that peaks in overvoltage are causally correlated to SoCs at which the various graphite stages take place (Fig. 7a and b, and Table 3). In the meantime that phase transitions take place, the overvoltage increases to a local maxima until the pure phase dominates. At the beginning of the next phase formation, we find a decrease in overvoltage (Fig. 7a and b).

In the particular case of graphite, phase transitions can be solid-solution phase transitions or they can undergo phase separation [22]. The phase transitions that show larger peaks at the incremental capacity curve, which are the transitions 1–2, 2-2L, and 4L-1L (Fig. 7a), undergo phase separation whereas the rest are related to solid-solution phase transitions [22].

With respect to positive electrode, it is composed of $LiCoO_2$—Li(NiMnCo)O_2 that is a combination of solid solutions of $LiCoO_2$ (LCO), $LiMnO_2$ (LMO) and $LiNiO_2$ (LNO). Its performance in Li-ion cells depends on the ratio between nickel, manganese and cobalt [52–55]. Furthermore, phase transitions and the formation of pure phases during lithiation or delithiation also depend strongly on the ratio between the composing metals as well as their synthetization [54]. Unfortunately, we do not have information about the exact composition of the electrode.

At the incremental capacity curves of the positive electrode of the fresh half-cell, four peaks related to phase transitions are identified (Fig. 7c). The correct assignment of a real phase transitions in SoC around 72% is challenging because we measure a very small variation. In the IC curve of the aged electrode (Fig. 7d), this variation is even smaller. Therefore, it might be that actually there is no phase transition associated to this particular SoC or that it does not take place in the aged electrode. In any case, we cannot assure it only from these measurements.

In the positive electrode, a peak in overvoltage is found after each of the phase transitions as well as in the negative electrode. However, at SoCs around 40% in the fresh electrode there is a local maximum in overvoltage that apparently has no related peak in the incremental capacity (Fig. 7c). Actually, we assume that the largest peak in the incremental capacity curve, which is centered at SoCs around 36%, might be hiding the peak that would be related to this overvoltage. However, we cannot affirm from our results that this peak in overvoltage truly corresponds to a phase transformation. The same peak around 40% SoC is found in the aged electrode (Fig. 7d). Moreover, an additional overvoltage peak is located around 20% in the aged cell. In contrast to the overvoltage peak at 40% SoC, the additional peak found at 20% has a direct correspondence with a new peak in the IC curve of the aged cell.

Concerning the full cell, all the overvoltage contributions observed in the half-cells (Fig. 7a-d) are also appreciable at the full-cell overvoltage (Fig. 7e and f). Nonetheless, incremental capacity curves do not show a direct correspondence between phase transitions taking place at positive and negative electrodes and the full cell. Here, it is also observed that towards the end of each phase transition there is always an increase in overvoltage (Fig. 7e and f), which has been previously assigned to concentration polarization (refer to Section 3.2).

The local maxima in overvoltage coincide with the formation of pure phases from which the overvoltage starts decreasing and continues doing it at the first stages of the new phase formation. In fact, at the

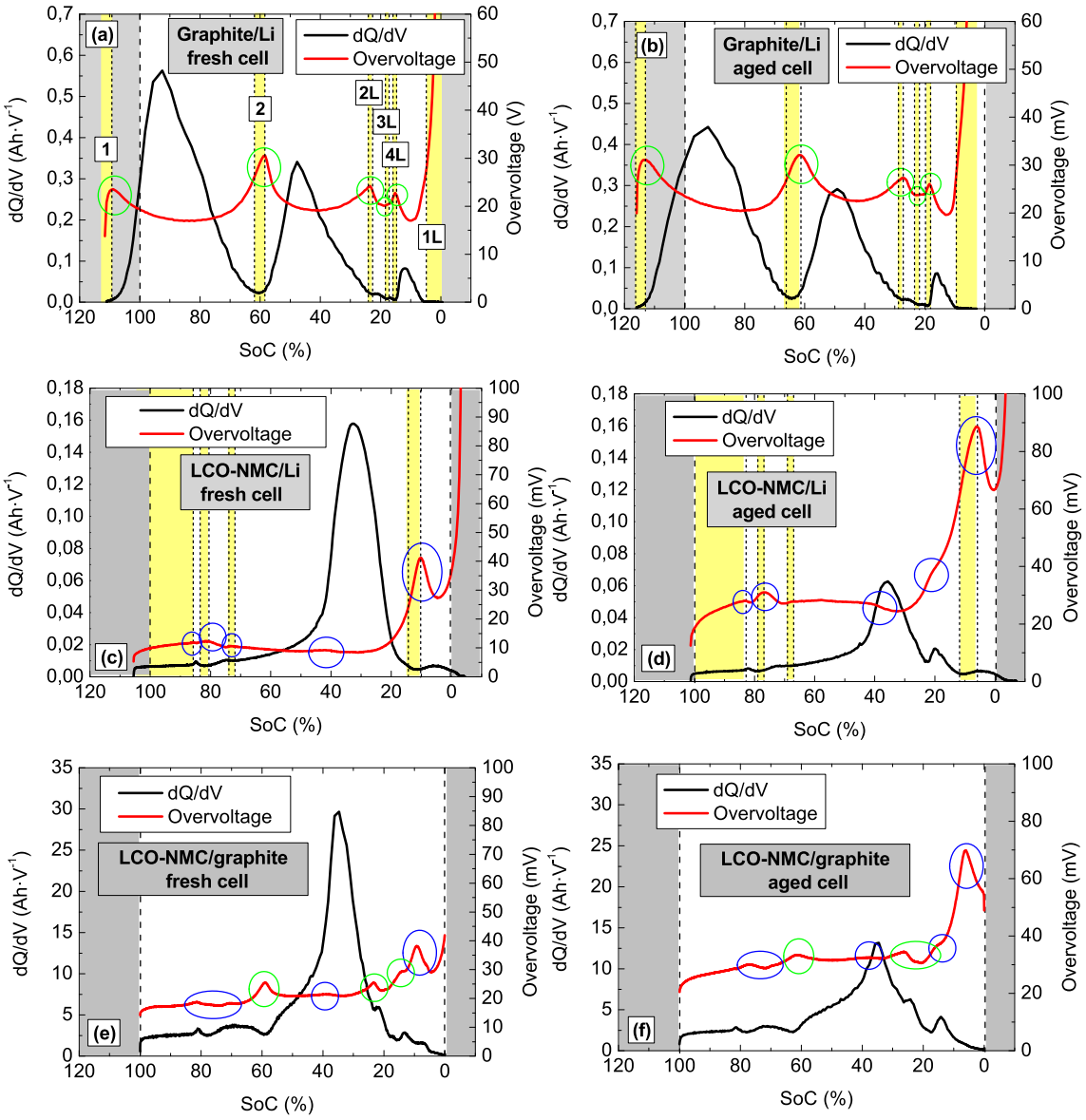

Fig. 7. Incremental capacity analysis and overvoltage generated in (a) fresh graphite/Li half-cell, (b) aged graphite/Li half-cell, (c) fresh LCO-NMC/Li half-cell, (d) aged LCO-NMC/Li half-cell, (e) fresh LCO-NMC/graphite full cell and (f) aged LCO-NMC/graphite full cell. The results are obtained during discharge (lithiation of positive electrode and delithiation of negative electrode) of fresh cells at a rate of C/25 at room temperature. Dashed lines separate phase transitions (white areas) from pure phases (yellow areas). Gray areas represent SoCs that were not considered in the full cells. (For interpretation of the references to colour in this figure legend, the reader is referred to the Web version of this article.)

Table 3
State-of-Charge associated to graphite stages 1, 2, 2L, 3L, 4L, and 1L during delithiation. Comparison is made between the results found in literature [22] and the ones obtained in this study by means of fresh half-cells.

Stages	1	2	2L	3L	4L	1L
SoC range in Ref. [22] [%]	95–100	50–53	30	20	12–13	0–5
NE SoC of local maxima in overvoltage [%]	97.5	52.8	21.1	18	13.5	6

beginning of a stage transition, the measured overvoltage reflects the processes of the new phase even though there is almost only the previous phase [22]. Therefore, as concentration gradients are not going to form until sometime after the initial formation of the new phase, initial SoCs of this phase transformation are not going to be affected by diffusion [22]. Thus, it might explain the decrease in concentration polarization that we find at these particular SoCs. Hess also state a relation between diffusion and overvoltage even though their results do not show the SoC dependency of overvoltage but they are obtained at various current rates and at particular SoCs [22]. Thus, we present novel experimental results of the diffusion SoC dependency of each of the phase transitions. Despite the fact that these results are not commonly found in the literature, our results are supported by other approximations in which diffusion coefficients are related to phase transitions at different SoCs [22,26,56,57]. Concerning the variability of diffusion with aging or the rate, we conclude from our results that when the cells age or are discharged at high rates, they are more affected by diffusion already from early stages of phase transitions.

Incremental capacity curves provide relevant information about the phase transitions and the formation of solid phases in the cells during lithiation and delithiation. Indeed, in this sense, they are very useful for half-cell measurements. However, as we can observe in Fig. 7, not all the phase transitions occurring at the half-cells can be identified at the full cells. For instance, this is the case of the peak associated with the

phase transition between stages 1 and 2 at the negative electrode, which is located around the 60% SoC (Fig. 7a) but cannot be appreciated at the full cell incremental capacity (Fig. 7e). In contrast, the peak in overvoltage generated during this particular phase transition can be identified at both the full cell and the half-cell overvoltages (Fig. 7a and e). Therefore, we find more convenient to evaluate changes in the structure of the cells with overvoltage measurements, which show to be more appropriate in the study of the formation of pure phases and the corresponding phase transitions during galvanostatic discharge of a complete cell.

Another advantage of our overvoltage analysis and its relationship with phase transitions is that the working SoC range can be optimized. The electrodes suffer high stress and volume changes during lithium insertion and extraction, what is reflected in the generated overvoltage. Thus, the overvoltage is a very valuable tool to make decisions about the SoCs that should be avoided. For instance, at positive electrode, SoCs below 15% are highly deteriorated during the aging process (Fig. 6). Therefore, a strategy to extend the lifecycle of the cells would be to avoid the SoCs below 15% in the discharge process. In the literature, it is common to find studies in which the effect of the charge/discharge SoC range in the capacity fade estimation is considered [58–60]. However, empirical relations are commonly obtained [58,59]. Nevertheless, we find that the results obtained by incremental capacity analysis are sometimes related to the charge/discharge SoC range [60]. Thus, from our results, we suggest that it would be more appropriate to determine the working SoC range from the evaluation of the various phase changes rather than choosing random SoCs to get empirical relations. Moreover, we propose to replace incremental capacity analysis by overvoltage analysis, if the phase transformations of the full cell are aimed to be indexed.

4. Conclusions

We evaluated the overvoltage that is produced in a Li-ion cell composed of LCO-NMC and graphite electrodes. The ohmic drop, activation, and concentration polarizations were quantified from voltage and impedance measurements. We found that concentration polarization dominates the voltage loses at low discharge rates whereas ohmic contribution, and more particularly the ionic conduction of the electrolyte, dominates the losses at high rates.

During galvanostatic discharge, we observed that concentration polarization can increase or decrease depending on the state of charge of the cell. From half-cell measurements, a relationship between phase transitions and the produced overvoltage was determined. An increase in overvoltage was produced towards the last stages of phase transitions whereas a decrease in overvoltage was produced at the first stages of new phases, which was attributed to the lack of diffusion limitations at the initial SoCs of the new phase. We determined that, considering those results, an optimized charging/discharging strategy could be defined.

Incremental capacity analysis was carried out to the half-cells and the full cell in order to study the various phase transitions. The results were compared to the measured overvoltage. This comparison showed that useful information about phase transitions could be extracted from full-cell overvoltage measurements at SoCs at which incremental capacity did not provide any information. Thus, making more appropriate to evaluate or track the SoC evolution of phase transitions by measuring the full cell overvoltage.

Acknowledgments

This work was supported by the Spanish Government MINECO/FEDER project [TEC2015-63899-C3-1-R]; and the Spanish Ministry of Education, Culture, and Sport [grant number FPU12/02603].

We are also very grateful to the Electrochemical Energy Conversion and Storage Systems Group from the Institute for Power Electronics and Electrical Drives (ISEA) for sharing their knowledge about post-mortem analysis and for letting us to carry out the tests at their Institution.

In addition, we also want to acknowledge the Hawaii Natural Energy Institute (HNEI), for giving us the possibility to use their facilities for cycling the cells and for carrying out the impedance measurements.

References

[1] M. Berecibar, I. Gandiaga, I. Villarreal, N. Omar, J. Van Mierlo, P. Van Den Bossche, Critical review of state of health estimation methods of Li-ion batteries for real applications, Renew. Sustain. Energy Rev. 56 (2016) 572–587, https://doi.org/10.1016/j.rser.2015.11.042.

[2] M. Murnane, A. Ghazel, A Closer Look at State of Charge (SOC) and State of Health (SOH) Estimation Techniques for Batteries, Analog Devices, n.d. http://www.analog.com/media/en/technical-documentation/technical-articles/A-Closer-Look-at-State-Of-Charge-and-State-Health-Estimation-Techniques-....pdf (accessed July 3, 2017).

[3] J. Jiang, C. Zhang, Fundamentals and Applications of Lithium-Ion Batteries in Electric Drive Vehicles, John Wiley & Sons, 2015.

[4] J.S. Newman, K. Thomas-Alyea, Electrochemical Systems, J. Wiley, 2004.

[5] D. Linden, T.B. Reddy, Handbook of Batteries, McGraw-Hill, 2001, https://doi.org/10.1016/0378-7753(86)80059-3.

[6] A. Ter Heijne, O. Schaetzle, S. Gimenez, F. Fabregat-Santiago, J. Bisquert, D.P.B.T.B. Strik, F. Barrière, C.J.N. Buisman, H.V.M. Hamelers, Identifying charge and mass transfer resistances of an oxygen reducing biocathode, Energy Environ. Sci. 4 (2011) 5035, https://doi.org/10.1039/c1ee02131a.

[7] J. Zhou, D. Danilov, P.H.L. Notten, A novel method for the in situ determination of concentration gradients in the electrolyte of Li-ion batteries, Chem. Eur J. 12 (2006) 7125–7132, https://doi.org/10.1002/chem.200600193.

[8] M.M. Khonsari, M. Amiri, Introduction to Thermodynamics of Mechanical Fatigue, CRC Pr I Llc, 2012.

[9] I. Kondepudi, Dilip, Prigogine, Modern Thermodynamics. From Heat Engines to Dissipative Structures, (1998).

[10] M. Amiri, M. Modarres, An entropy-based damage characterization, Entropy 16 (2014) 6434–6463, https://doi.org/10.3390/e16126434.

[11] R. Chandrasekaran, Quantification of contributions to the cell overpotential during galvanostatic discharge of a lithium-ion cell, J. Power Sources 262 (2014) 501–513, https://doi.org/10.1016/j.jpowsour.2014.03.124.

[12] I.H. Buchberger, Electrochemical and Structural Investigations on Lithium-Ion Battery Materials and Related Degradation Processes, Technischen Universität München, 2016.

[13] R. Shekhar, Activation Overpotential, Indian Institute of Technology, (n.d).

[14] T.-R. Yu, G.L. Ji, Electrochemical Methods in Soil and Water Research, Pergamon Press, 1993.

[15] J. Illig, Physically Based Impedance Modelling of Lithium-Ion Cells, KIT Scientific Publishing, 2014, https://doi.org/10.5445/KSP/1000042281.

[16] E.J. Calvo, The current-potential relationship, Encycl. Electrochem, Wiley-VCH Verlag GmbH & Co. KGaA, Weinheim, Germany, 2007, pp. 3–30, , https://doi.org/10.1002/9783527610426.bard020101.

[17] C. Breitkopf, K. Swider-Lyons, Springer Handbook of Electrochemical Energy, (2017), https://doi.org/10.1007/978-3-662-46657-5.

[18] F. Béguin, E. Frąckowiak, Carbons for Electrochemical Energy Storage and Conversion Systems, CRC Press, 2009.

[19] B. Saha, P. Quach, K. Goebel, Exploring the model design space for battery health management, Annu. Conf. Progn. Heal. Manag. Soc. (2011) 1–8.

[20] J. Xu, R.D. Deshpande, J. Pan, Y.-T. Cheng, V.S. Battaglia, Electrode side reactions, capacity loss and mechanical degradation in lithium-ion batteries, J. Electrochem. Soc. 162 (2015) A2026–A2035, https://doi.org/10.1149/2.0291510jes.

[21] Y.H. Kao, M. Tang, N. Meethong, J. Bai, W.C. Carter, Y.M. Chiang, Overpotential-dependent phase transformation pathways in lithium iron phosphate battery electrodes, Chem. Mater. 22 (2010) 5845–5855, https://doi.org/10.1021/cm101698b.

[22] M. Hess, Kinetics and Stage Transitions of Graphite for Lithium-Ion Batteries, (2013), https://doi.org/10.3929/ethz-a-010000442.

[23] T.R. Ferguson, M.Z. Bazant, Phase transformation dynamics in porous battery electrodes, Electrochim. Acta 146 (2014) 89–97, https://doi.org/10.1016/j.electacta.2014.08.083.

[24] P. Bai, D. a Cogswell, M.Z. Bazant, Suppression of phase separation in $LiFePO_4$ nanoparticles during battery discharge, Nano Lett. 11 (2011) 4890–4896, https://doi.org/10.1021/nl202764f.

[25] C. Liu, Z.G. Neale, G. Cao, Understanding electrochemical potentials of cathode materials in rechargeable batteries, Mater. Today 19 (2016) 109–123, https://doi.org/10.1016/j.mattod.2015.10.009.

[26] M. Tang, W.C. Carter, Y.-M. Chiang, Electrochemically driven phase transitions in insertion electrodes for lithium-ion batteries: examples in lithium metal phosphate Olivines, Annu. Rev. Mater. Res. 40 (2010) 501–529, https://doi.org/10.1146/annurev-matsci-070909-104435.

[27] M.Z. Bazant, Theory of chemical kinetics and charge transfer based on nonequilibrium thermodynamics, Acc. Chem. Res. 46 (2013) 1144–1160, https://doi.org/10.1021/ar300145c.

[28] Y. Merla, B. Wu, V. Yufit, N.P. Brandon, R.F. Martinez-Botas, G.J. Offer, Novel application of differential thermal voltammetry as an in-depth state-of-health diagnosis method for lithium-ion batteries, J. Power Sources 307 (2016) 308–319,

https://doi.org/10.1016/j.jpowsour.2015.12.122.
[29] M. Dubarry, C. Truchot, B.Y. Liaw, Synthesize battery degradation modes via a diagnostic and prognostic model, J. Power Sources 219 (2012) 204–216, https://doi.org/10.1016/j.jpowsour.2012.07.016.
[30] Z. Wang, Z. Wang, W. Peng, H. Guo, X. Li, J. Wang, A. Qi, Structure and electrochemical performance of $LiCoO_2$ cathode material in different voltage ranges, Ionics 20 (2014) 1525–1534, https://doi.org/10.1007/s11581-014-1098-z.
[31] D.D.E.R. Wissenschaften, F.L.A. Mantia, Characterization of Electrodes for Lithium-Ion Batteries through Electrochemical Impedance Spectroscopy and Mass Spectrometry, (2008).
[32] P.G. Bruce, Solid-state chemistry of lithium power sources, Chem. Commun. (1997) 1817–1824, https://doi.org/10.1039/a608551b.
[33] P. Hou, G. Chu, J. Gao, Y. Zhang, L. Zhang, Li-ion batteries: phase transition, Chin. Phys. B 25 (2016) 1–11, https://doi.org/10.1088/1674-1056/25/1/016104.
[34] V.J. Ovejas, Determination of the State of Health of Li-Ion Batteries: the Irreversible Entropy Production Approach, Universitat Politècnica de Catalunya, 2017.
[35] M. Dubarry, B.Y. Liaw, Identify capacity fading mechanism in a commercial $LiFePO_4$ cell, J. Power Sources 194 (2009) 541–549, https://doi.org/10.1016/j.jpowsour.2009.05.036.
[36] V.J. Ovejas, A. Cuadras, Impedance characterization of an LCO-NMC/graphite cell: Ohmic conduction, SEI transport and charge-transfer phenomenon, Batteries 4 (3) (2018) 43, https://doi.org/10.3390/batteries4030043.
[37] K.A. Natarajan, Exchange current density – polarization relationships lecture 9 (2015), pp. 1–6 2 http://nptel.ac.in/courses/113108051/module2/lecture9.pdf , Accessed date: 28 May 2017.
[38] C. Lim, M.Z. Bazant, Reaction Kinetics Lecture 13 : Butler-Volmer Equation, MIT OpenCourseWare., 2014, http://ocw.mit.edu , Accessed date: 10 January 2018.
[39] J. Garche, C.K. Dyer, Encyclopedia of Electrochemical Power Sources, Academic Press, 2009.
[40] M. Klett, R. Eriksson, J. Groot, P. Svens, K. Ciosek Högström, R.W. Lindström, H. Berg, T. Gustafson, G. Lindbergh, K. Edström, Non-uniform aging of cycled commercial $LiFePO_4$//graphite cylindrical cells revealed by post-mortem analysis, J. Power Sources 257 (2014) 126–137, https://doi.org/10.1016/j.jpowsour.2014.01.105.
[41] A. Anderson, Surface Phenomena in Li-Ion Batteries, Uppsala University, 2001, https://doi.org/10.1149/1.1393357.
[42] J.S. Gnanaraj, Y.S. Cohen, M.D. Levi, D. Aurbach, The effect of pressure on the electroanalytical response of graphite anodes and $LiCoO_2$ cathodes for Li-ion batteries, J. Electroanal. Chem. 516 (2001) 89–102, https://doi.org/10.1016/S0022-0728(01)00663-5.
[43] M. Dubarry, V. Svoboda, R. Hwu, B.Y. Liaw, Capacity and power fading mechanism identification from a commercial cell evaluation, J. Power Sources 165 (2007) 566–572, https://doi.org/10.1016/j.jpowsour.2006.10.046.
[44] W. Waag, C. Fleischer, D.U. Sauer, Critical review of the methods for monitoring of lithium-ion batteries in electric and hybrid vehicles, J. Power Sources 258 (2014) 321–339, https://doi.org/10.1016/j.jpowsour.2014.02.064.
[45] F. Yue, G. Zhang, J. Zhang, J. Lin, K. Jiao, Numerical simulation of transport characteristics of Li-ion battery in different discharging modes, Appl. Therm. Eng. 126 (2017) 70–80, https://doi.org/10.1016/j.applthermaleng.2017.07.151.
[46] J. Sun, G. Wei, L. Pei, R. Lu, K. Song, C. Wu, C. Zhu, Online internal temperature estimation for lithium-ion batteries based on Kalman filter, Energies 8 (2015) 4400–4415, https://doi.org/10.3390/en8054400.
[47] D.J. Xiong, T. Hynes, J.R. Dahn, Dramatic effects of low salt concentrations on Li-ion cells containing EC-free electrolytes, J. Electrochem. Soc. 164 (2017) A2089–A2100, https://doi.org/10.1149/2.1381709jes.
[48] Bazant, Pseudocapacitors and batteries, MIT lect, (2011), pp. 1–12 https://ocw.mit.edu/courses/chemical-engineering/10-626-electrochemical-energy-systems-spring-2014/lecture-notes/MIT10_626S14_S11lec37.pdf , Accessed date: 2 June 2017.
[49] Y. Mnyukh, Mechanism and kinetics of phase transitions and other reactions in solids, Am. J. Condens. Matter. Phys. 3 (2011) 89–103, https://doi.org/10.5923/j.ajcmp.20130304.01.
[50] Y. Shao-Horn, Understanding phase transformations in lithium battery materials by transmission electron microscopy, Sci. Technol. Lithium Batter, Kluwer Academic Publishers, 2003, pp. 478–506, , https://doi.org/10.1007/978-0-387-92675-9_16.
[51] X.L. Wang, K. An, L. Cai, Z. Feng, S.E. Nagler, C. Daniel, K.J. Rhodes, A.D. Stoica, H.D. Skorpenske, C. Liang, W. Zhang, J. Kim, Y. Qi, S.J. Harris, Visualizing the chemistry and structure dynamics in lithium-ion batteries by in-situ neutron diffraction, Sci. Rep. 2 (2012) 751–767, https://doi.org/10.1038/srep00747.
[52] S. Liu, L. Xiong, C. He, Long cycle life lithium ion battery with lithium nickel cobalt manganese oxide (NCM) cathode, J. Power Sources 261 (2014) 285–291, https://doi.org/10.1016/j.jpowsour.2014.03.083.
[53] R. Amin, Y.-M. Chiang, Characterization of electronic and ionic transport in $Li_{1-x}Ni_{0.33}Mn_{0.33}Co_{0.33}O_2$ (NMC333) and $Li_{1-x}Ni_{0.5}Mn_{0.2}Co_{0.3}O_2$ (NMC523) as a function of Li, J. Electrochem. Soc. 163 (2016) 1512–1517, https://doi.org/10.1149/2.0131608jes.
[54] C. Julien, A. Mauger, K. Zaghib, H. Groult, Optimization of layered cathode materials for Lithium-Ion batteries, Materials 9 (2016) 595, https://doi.org/10.3390/MA9070595.
[55] Q. Wang, N. Tian, K. Xu, L. Han, J. Zhang, W. Zhang, S. Guo, C. You, A facile method of improving the high rate cycling performance of $LiNi_{1/3}Co_{1/3}Mn_{1/3}O_2$ cathode material, J. Alloy. Comp. 686 (2016) 267–272, https://doi.org/10.1016/j.jallcom.2016.06.017.
[56] M.D. Levi, E. Markevich, D. Aurbach, Comparison between Cottrell diffusion and moving boundary models for determination of the chemical diffusion coefficients in ion-insertion electrodes, Electrochim. Acta 51 (2005) 98–110, https://doi.org/10.1016/j.electacta.2005.04.007.
[57] J. Barker, R. Koksbang, M.Y. Saidi, An electrochemical investigation into the lithium insertion properties of LixNiO ($0 < x < 1$), Solid State Ionics 89 (1996) 25–35.
[58] P. Ramadass, B. Haran, P.M. Gomadam, R. White, B.N. Popov, Development of first principles capacity fade model for Li-ion cells, J. Electrochem. Soc. 151 (2004) A196, https://doi.org/10.1149/1.1634273.
[59] S. Saxena, C. Hendricks, M. Pecht, Cycle life testing and modeling of graphite/LiCoO2 cells under different state of charge ranges, J. Power Sources 327 (2016) 394–400, https://doi.org/10.1016/j.jpowsour.2016.07.057.
[60] A. Maheshwari, M. Heck, M. Santarelli, Cycle aging studies of lithium nickel manganese cobalt oxide-based batteries using electrochemical impedance spectroscopy, Electrochim. Acta 273 (2018) 335–348, https://doi.org/10.1016/j.electacta.2018.04.045.

Glossary

CC: Current Collector
CT: Charge Transfer
ICA: Incremental Capacity Analysis
LCO: Lithium Cobalt Oxide
Li-ion: Lithium ion
LMO: Lithium Manganese Oxide
LNO: Lithium Nickel Oxide
NE: Negative Electrode
NMC: Lithium Nickel Manganese Cobalt Oxide
OCV: Open Circuit Voltage
PE: Positive Electrode
Ps-OCV: Pseudo Open Circuit Voltage
SEI: Solid Electrolyte Interface
SoC: State-of-Charge
SoH: State-of-Health